Biomass Conversion and Biorefinery (2024) 14:4355–4368
https://doi.org/10.1007/s13399-022-02464-7

ORIGINAL ARTICLE

Removal of Cr(VI) by iron nanoparticles synthesized by a novel green method using Yali pear peels extracts: optimization, reactivity, and mechanism

Kun Rong[1,2] · Jinye Wang[1] · Xueping Li[2] · Zaiwang Zhang[2] · ·Qian Yang[2] · ·Changqing Shan[2] · Tao Wu[2] · Juanjuan Liu[2]

Received: 12 January 2022 / Revised: 9 February 2022 / Accepted: 10 February 2022 / Published online: 4 March 2022

Abstract

In recent years, the removal of hexavalent chromium by green iron nanoparticles (FeNPs) has attracted attention due to the environmental friendliness, low price, and good durability of this adsorbent. In this paper, a new synthetic method was developed and optimized under the aspects of improved synthesis yield and Cr(VI) removal. For the first time, peel extracts of yali pear and $FeSO_4$ were employed in the synthesis of FeNPs (YL-FeNPs), and the synthesis conditions were optimized for five factors including extraction temperature, extraction time, peel mass, Fe^{2+}-extract ratio, and drying method. For optimized synthesis conditions, the following parameters were determined: 27 g of pear peel was extracted with 360 mL of 50 vol% ethanol solution in water at 80 °C for 60 min, the Fe^{2+}-extracts volume ratio was 1:1, and vacuum freeze drying was employed. The optimized YL-FeNPs formed particles of irregular shape with a size in the range of 40–80 nm. As the initial Cr(VI) concentration decreased and the adsorption temperature increased, its removal efficiency improved. After 2 h, a Cr(VI) removal efficiency of 96.8% was achieved for a solution with an initial Cr(VI) concentration of 12 mg/L. The adsorption of Cr(VI) conformed to pseudo-second-order kinetics and the Langmuir adsorption isotherm model. YL-FeNPs exhibited a maximum adsorption capacity of 43.99 mg/g at pH = 5 and 55 °C and demonstrated good adsorption performance in solutions with coexisting anions and real natural water. This research can support the recycling of pear peel waste and provide technical aspects for improving the synthesis efficiency of FeNPs.

Keywords Iron nanoparticles · Hexavalent chromium · Green synthesis · Optimization · Yali pear peel

1 Introduction

Chromium (Cr) pollution is frequently present in wastewater of the leather, electroplating, steel, and other industries [1–3]. Cr mainly appears in two forms, Cr(VI) and Cr(III), of which the toxicity and solubility of Cr(VI) are much higher than those of Cr(III). Hexavalent chromium requires treatment as it threatens ecological environment and the human health [4]. The adsorption method is widely used in the Cr(VI) removal mainly because of its easy operation. Iron nanoparticles (FeNPs) are one of the most widely used repair agents in the adsorption method [5–8]. In the traditional chemical synthesis method using sodium borohydride for the preparation of FeNPs, toxic substances are employed or produced, and energy consumption is high. Green synthesis methods of nanomaterials use natural materials such as plants and microorganisms to synthesize the materials and possess the advantages of environmental friendliness, fast synthesis, and possible resource recycling [9]. Previously, banana peel [10], pomegranate peel [11], tangerine peel [12], lemon peel [13], apple peel [14], and the leaves of a variety of plants [15] were used to synthesize FeNPs, which were employed for the pollutants removal in water.

To improve the application advantages of green FeNPs and reduce preparation cost, many scholars have optimized the synthesis method of FeNPs. The effects of extraction time, extraction temperature, and leaf-water ratio on the

✉ Jinye Wang
2005010@glut.edu.cn

[1] College of Environmental Science and Engineering, Guilin University of Technology, 319 Yanshan Street, Yanshan, Guilin 541006, People's Republic of China

[2] Shandong Engineering and Technology Research Center for Ecological Fragile Belt of Yellow River Delta, Binzhou University, 391 Huanghe 5th Rd, Bincheng District, Binzhou 256600, People's Republic of China

antioxidant properties of the extract were studied in the water extraction of *Amaranthus dubius* leaves [16]; a greater FeNP yield could be achieved when high-concentration extract and iron(III) chloride ($FeCl_3$) were used for the synthesis. Liu [17] studied the effect of temperature in the extraction of *Eucalyptus* leaves on the removal of hexavalent chromium and found the highest removal efficiency for the FeNPs prepared from the extract obtained at an extraction temperature of 80 °C. During the process of using fresh *Mentha piperita* leaves and $FeCl_3$ to synthesize FeNPs [18], the particle size of FeNPs was the smallest when the Fe^{3+}-extract volume ratio was 1:1.5. Some scholars have used *Eichhornia crassipes* leaf extract [19] or *Citrus maxima* bark extract [20] and $FeCl_3$ to synthesize FeNPs and studied the effect of Fe^{3+}-extract ratio on Cr(VI) removal by the prepared FeNPs. The optimal Fe^{3+}-extract volume ratio was finally set as 1:1 and 1:3. FeNPs synthesized from red peanut peel extract and $FeCl_3$ exhibited a much smaller particle size when applying vacuum drying compared to air drying [21].

In studies on the synthesis and optimization of FeNPs, the Cr(VI) removal efficiency of FeNPs synthesized with $FeCl_3$ increased with the increase in the volume of the extract [19, 20] because the extract but not Fe^{3+} contributes to the removal of Cr(VI) [19]. The removal efficiency of heavy metals by FeNPs synthesized with $FeCl_3$ [17] and iron(II) sulfate ($FeSO_4$) [22] first increased and then decreased as the volume of the extract increased. With continuing increase in the volume of the extract, the excess biomass coated on FeNPs increased the particle size and reduced the activity of FeNPs [23]. The Cr(VI) removal efficiency of FeNPs synthesized with $FeSO_4$ decreased with increasing volume of the extract [24], while the removal efficiency of methyl orange increased [25]. The published results indicate that the optimal Fe^{3+}-extract ratio was affected by various factors such as the extract composition, experimental methods, and target pollutants, and the main control mechanism may differ in the different experiments. In addition, previous studies focused more on the removal efficiency of pollutants, and less research concentrated on the yield of FeNPs. Few studies were conducted on the effect of extraction time and temperature of the plant extracts on the performance of FeNPs. Therefore, to optimize the synthesis method of FeNPs, starting with the characteristics of the extract itself is required, both removal efficiency of pollutants and yield of FeNPs need to be considered, and the optimization of the synthesis conditions has to include the extraction time and temperature of the extract to improve the comprehensive performance of FeNPs.

Yali pear (*Pyrus bretschneideri* Rehd.) is harvested in large yields in Binzhou City, Shandong Province, China. Yangxin County in Binzhou City is the "hometown of Yali pears in China," and Binzhou City is a rich source of Yali pear peel. The polyphenols contained in pear peel [26] provide the possibility for green synthesis of FeNPs. However, only few studies were published on the green synthesis of FeNPs with Yali pear peel extracts. In this paper, peel extracts of Yali pears were used to prepare FeNPs, and the improvement of the synthesis method was studied. The main goals of this paper are as follows: (1) The synthesis conditions were optimized for the parameter extraction temperature, extraction time, and Fe^{2+}-extract ratio to improve the removal efficiency of Cr(VI) as well as the yield of FeNPs. (2) The optimized YL-FeNPs were characterized by various test methods, and the particle size, structure, and composition of YL-FeNPs were analyzed. (3) The effects of adsorption time, initial concentration, presence of different anions, and use of real water on Cr(VI) removal as well as on adsorption isotherms and kinetics were studied to explore the mechanism of hexavalent chromium removal by FeNPs. This research can support the recycling of pear peel waste and provide technical aspects for improving the green synthesis conditions of FeNPs.

2 Materials and methods

2.1 Materials

Fresh Yali pears were purchased in a store in Binzhou City, Shandong Province, China. Iron(II) sulfate heptahydrate ($FeSO_4{\cdot}7H_2O$), ethanol (C_2H_6O), potassium chromate ($K_2Cr_2O_7$), and 1,5-diphenylcarbazide ($C_{13}H_{14}N_4O$) were purchased from Sinopharm Chemical Reagent Company, Ltd. (China). The chemicals used in the experiments were analytically pure and used without further purification. Aqueous solutions and pear peel extracts were prepared with deionized water.

2.2 Synthesis procedure of YL-FeNPs

The standard method for preparing YL-FeNPs is as follows: A Yali pear was washed, and a certain amount of chopped pear peel was added to 360 mL of 50 vol% ethanol solution in water. The mixture was stirred and heated in a water bath at 80 °C for 80 min. The produced liquid was then filtered in a vacuum to obtain the pear peel extract filtrate. An aqueous 0.1-M $FeSO_4$ solution and the extract were mixed in a volume ratio of 1:2 and heated under stirring in a water bath at 40 °C for 30 min. The obtained FeNP suspension was centrifuged for 8 min at a speed of 10,000 r/min in a refrigerated centrifuge. The FeNPs were dried at 60 °C with a hot-air dryer. The resulting material was called Yali-iron nanoparticles (YL-FeNPs).

In the process of using $FeSO_4$ solution and the extract to synthesize FeNPs, Fe^{2+} was reduced to Fe^0 by polyphenols

present in the extract. The synthesis mechanism of FeNPs [15] is shown in Eq. (1):

$$nFe^{2+} + 2Ar - (OH)_n \rightarrow nFe^0 + 2nAr = O + 2nH^+ \quad (1)$$

In Eq. (1), n means the number of hydroxyl (− OH) oxidized by Fe^{2+}, and Ar means the polyphenol aromatic ring.

2.3 Peel extract optimization

Based on the preparation method of YL-FeNPs in part 2.2, the following parameters for pear peel extraction that affected Cr(VI) removal were optimized: extraction temperature, extraction time, and peel mass. In the experiments, the extraction temperature was set to 50, 60, 70, 80, and 90 °C, and the effects of the extraction temperature on the yield of YL-FeNPs and the removal efficiency of Cr(VI) were studied. The yield of YL-FeNPs was calculated by using the solid mass (g) of YL-FeNPs obtained after centrifugation and drying per 375 mL of YL-FeNP suspension as the standard. Extraction time was set to 20, 40, 60, 80, and 100 min. Peel mass was set to 7, 13.5, 20, 27, 36, 40.5, 47, and 54 g per 360 mL of the ethanol–water mixture. In the Cr(VI) removal experiments, 0.02 g YL-FeNPs prepared under each synthesis condition was added to 50 mL of Cr(VI) solution for 120-min adsorption experiments, and the removal effect of different YL-FeNP materials was compared to optimize the pear peel extraction conditions for maximal Cr(VI) removal efficiency.

2.4 Optimization of YL-FeNPs synthesis

After the optimization of pear peel extraction in part 2.3 was completed, the synthesis conditions of YL-FeNPs that affected the removal of Cr(VI) were further optimized, which consisted of the volume ratio of the Fe^{2+} solution and the extract as well as the drying method. In the experiment, aqueous 0.1-M $FeSO_4$ solution was selected as Fe^{2+} source, and the used extracts were optimized extracts. When the volume ratio was optimized, the total volume of both solutions was fixed to 375 mL, and the volume ratio of Fe^{2+} solution and extract was set to 3:1, 2:1, 1:1, 2:3, 1:2, 1:3, and 1:5. The effects of the volume ratio on the yield of YL-FeNPs and the removal efficiency of Cr(VI) were studied. The method of calculating the yield of YL-FeNPs was the same as in Sect. 2.3. The tested drying methods included vacuum freeze drying at − 50 °C, vacuum drying at 60 °C, and hot-air drying at 60 ℃ for 10 h. The Cr(VI) removal efficiencies of 0.02 g YL-FeNPs were compared to optimize the synthesis conditions of YL-FeNPs.

2.5 Characterization of YL-FeNPs

The optimized YL-FeNPs were characterized by various test methods. The form, dispersion, and size of YL-FeNPs were analyzed by TEM (FEI Tecnai G2F30, USA). The surface of YL-FeNPs before and after Cr(VI) adsorption was analyzed by SEM (Hitachi SU8020, Japan). The functional groups of the compounds in the extracts and on the surface of YL-FeNPs before and after Cr(VI) adsorption were analyzed by FTIR (Nicolet IS10, USA) and compared. The structure of YL-FeNPs was analyzed by XRD (Brucker-D8 Advance, Germany). The valence state of Fe in YL-FeNPs was analyzed by XPS (Thermo Scientific Escalab 250Xi, USA).

2.6 *Cr(VI)* removal

The effects of contact time (0–180 min), initial Cr(VI) concentration (10–-80 mg/L), coexisting anions (NO_3^-, Cl^-, PO_4^{3-}, CO_3^{2-}, SO_4^{2-}), and real water bodies (river and tap water) on Cr(VI) removal were studied. The investigation included adsorption kinetics and adsorption isotherms. Finally, based on the characterization results, adsorption kinetics, and previous results, the reaction mechanism was analyzed. UV–Vis spectrophotometry (Purkinjie General AU-1901, China) was used to determine the Cr(VI) concentration using the 1,5-diphenylcarbazide method at 540 nm [1–4]. The removal efficiency R (%) of hexavalent chromium was determined using the equation:

$$R(\%) = (C_0 - C_t)/C_0 \times 100\% \quad (2)$$

Here C_0 and C_t are the concentrations at time zero and t, respectively (mg/L).

3 Results and discussion

3.1 Optimization of YL-FeNP synthesis

The relationship between extraction temperature and the removal efficiency of hexavalent chromium and the yield of YL-FeNPs is shown in Fig. 1. As the extraction temperature increased from 50 to 90 °C, the removal efficiency of Cr(VI) gradually improved, which might be attributed to an increased extraction rate of polyphenols at higher temperatures [27]. The result infers that the reaction (Eq. (1)) of YL-FeNP synthesis was more complete, resulting in greater amounts of Fe^0 in the material and, consequently, in greater Cr(VI) removal efficiency. Furthermore, the yield of YL-FeNPs did not change significantly with the increase in extraction temperature from 50 to 80 °C but dropped sharply with a further increase to 90 °C. As an explanation,

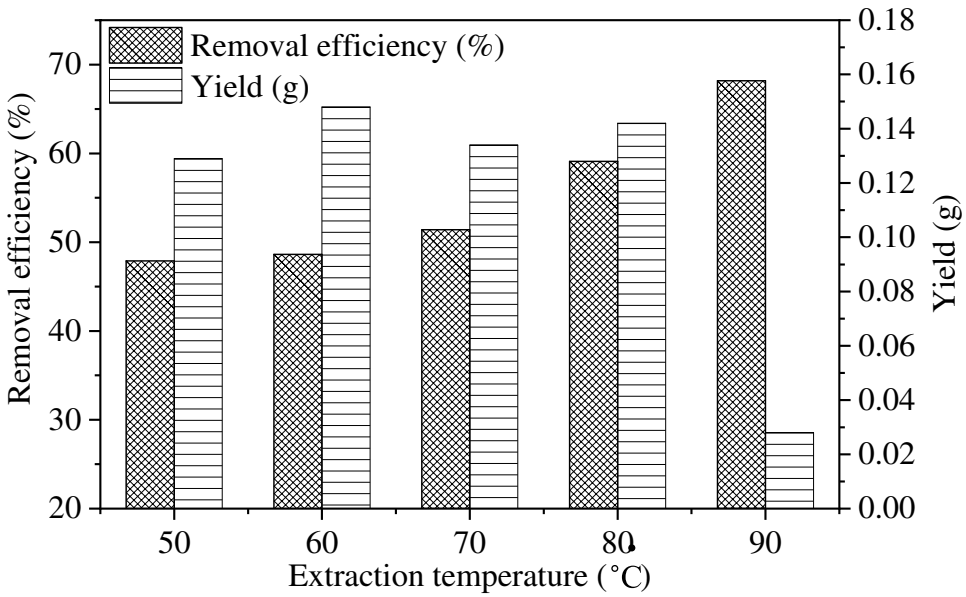

Fig. 1 Effect of extraction temperature at an extraction time of 80 min on Cr(VI) removal and YL-FeNP yield (Cr(VI) removal condition: 0.02 g YL-FeNPs, 55 °C, pH = 3, 20 mg/L initial Cr(VI) concentration)

the extract was subjected to serious evaporation at 90 °C, and its volume for the synthesis of YL-FeNPs was considerably reduced. In addition, the suspension of the YL-FeNPs synthesized from the extract obtained at 90 °C was difficult to separate by centrifugation, resulting in a sharp decrease in yield. Considering both Cr(VI) removal efficiency and YL-FeNP yield, the optimal extraction temperature was 80 °C.

Figure 2 shows the removal efficiency and YL-FeNP yield for different extraction times at the same extraction temperature of 80 °C. As the extraction time increased from 20 to 60 min, the removal efficiency increased by about 16% and remained basically stable with a further increase in extraction time to 100 min. Geng's research [26] showed that the extraction rate of polyphenols from pear peels reached the maximum at an extraction time of 60 min and did not increase with longer extraction times. Therefore, the observed stable removal efficiency after the extraction time reached 60 min might be related to Geng's results. Based on the removal efficiency of Cr(VI) and considering the cost of prolonged extraction time, it was concluded that the optimal extraction time was 60 min.

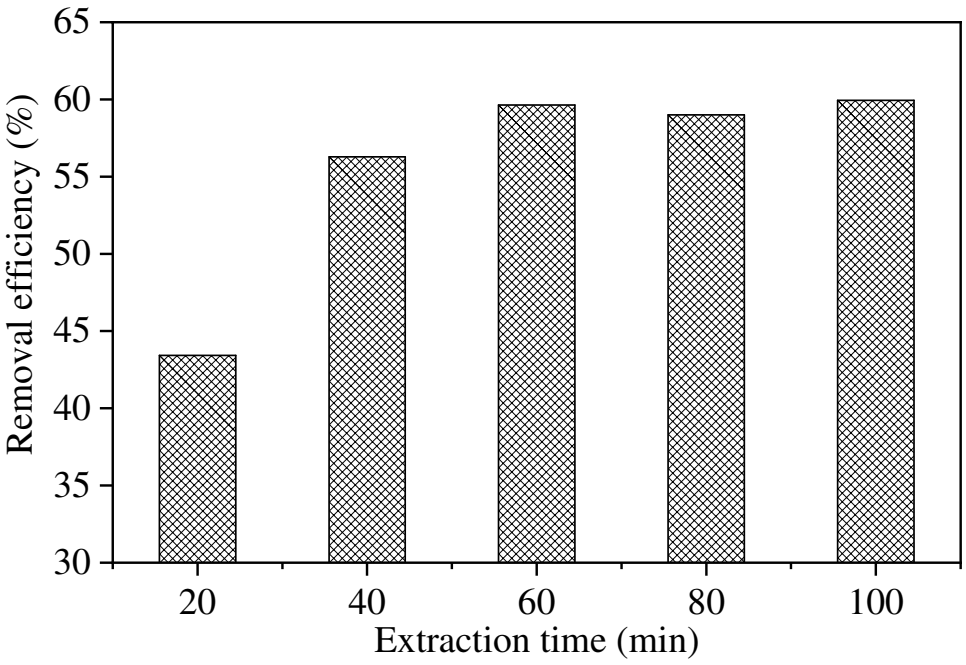

Fig. 2 Effect of extraction time at an extraction temperature of 80 °C on Cr(VI) removal (removal conditions are the same as stated in Fig. 1)

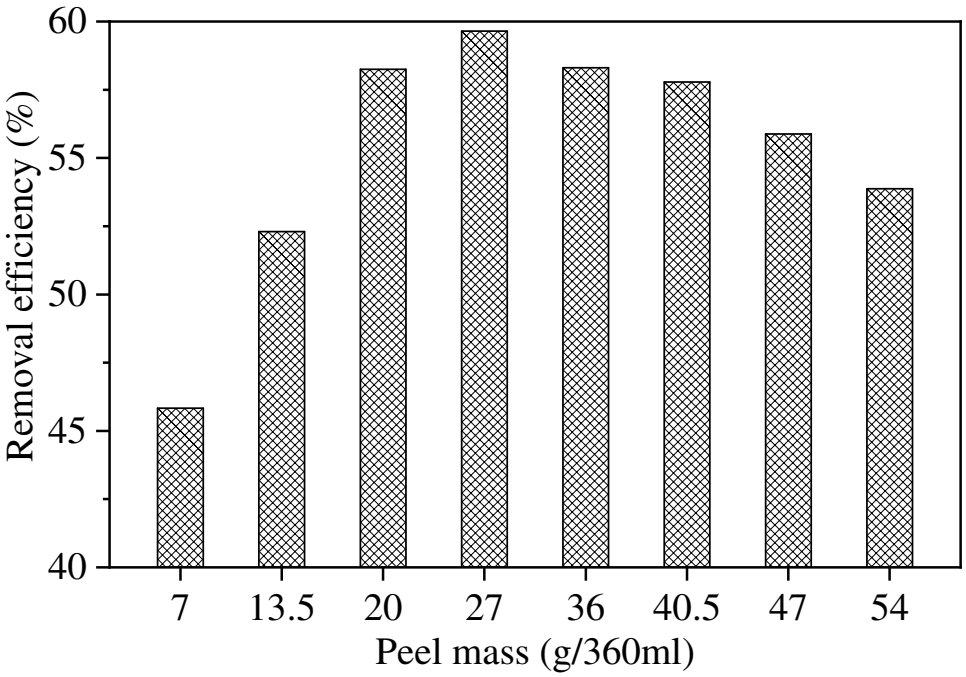

Fig. 3 Effect of peel mass on Cr(VI) removal (extraction temperature and time: 80 °C and 60 min; Cr(VI) removal conditions are the same as stated in Fig. 1)

The results on the influence of peel mass on the removal efficiency are displayed in Fig. 3. With increasing peel mass, Cr(VI) removal efficiency first rose and then decreased. When 27 g of pear peel was extracted by 360 mL of the ethanol–water mixture, the removal efficiency was the highest. This observation corroborates the result by Geng et al. [26] that, with increasing peel mass, the extraction rate of polyphenols first increased and then decreased. When raising the peel mass after the extraction rate of polyphenols reached the maximum, the impurities extracted from the pear peel may affect the synthesis of YL-FeNPs, thus reducing the removal efficiency of Cr(VI) per unit mass of FeNPs.

The effect of the Fe^{2+}-extract volume ratio on Cr(VI) removal efficiency and YL-FeNP yield is shown in Fig. 4. With increasing volume of extract, the removal efficiency of Cr(VI) gradually decreased. As an explanation, the polyphenols and other compounds in the extract not only acted as reducing agent but also as coating agent during the synthesis of YL-FeNPs. When the volume of extract continued to increase, a greater amount of biomass was present on the surface of YL-FeNPs, impeding the contact of Fe^0 and Fe^{2+} in YL-FeNPs with heavy metal ions [22]. In addition, the synthesized FeNPs exhibited a larger particle size, the activity was reduced [23], and consequently,

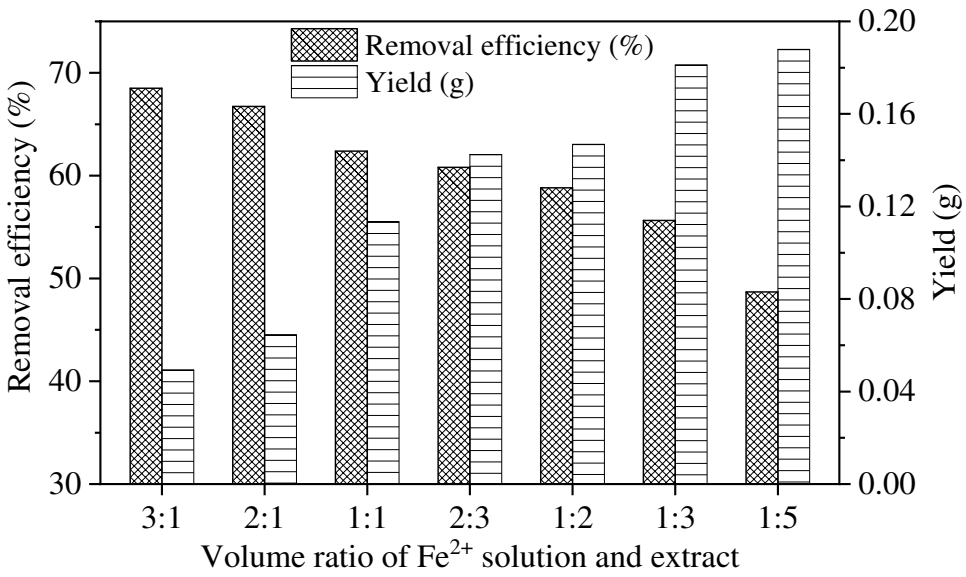

Fig. 4 Effect of volume ratio on Cr(VI) removal and YL-FeNP yield (extraction condition: 27 g/360 mL of extractant, 80 °C, 60 min; Cr(VI) removal conditions are the same as stated in Fig. 1)

the Cr(VI) removal efficiency declined. When using green tea extract and $FeSO_4$, Hao [24] also found that the removal efficiency of Cr(VI) decreased as the volume of the extract increased. In Fig. 4, the yield of YL-FeNPs prepared by 375 mL of a mixture of Fe^{2+} solution and extract gradually increases with the increase in extract volume fraction, which is consistent with the conclusion that the yield of SF-FeNPs increases with increasing volume of sunflower leaf extract [22]. In general, when the volume ratio of Fe^{2+} solution and extract was 1:1, the removal efficiency of Cr(VI) was higher, and the yield of YL-FeNPs was above average; therefore, the best volume ratio was 1:1.

The influence of the drying method applied in the YL-FeNP synthesis on the Cr(VI) removal efficiency is displayed in Fig. 5. The best efficiency was observed with the material prepared by vacuum freeze drying, and ordinary vacuum drying ranked second, while hot-air drying resulted in the lowest removal efficiency. Hot-air drying would cause Fe^0 on the surface of YL-FeNPs to be oxidized to Fe_3O_4, which not only reduced the content of Fe^0 and Fe^{2+} in FeNPs but also increased the particle size of FeNPs [21]; consequently, the removal efficiency of hot-air dried YL-FeNPs was lower than that of the vacuum-dried absorbents. The dispersibility of the material prepared by vacuum freeze drying was better than that of the material dried under ordinary vacuum [28], indicating an increased surface area of the adsorbent; therefore, the removal efficiency of the material dried by the vacuum freeze method was greater, which then constituted the best drying method.

3.2 Characterization of YL-FeNPs

YL-FeNPs were prepared using the above-optimized synthesis method and were characterized by various techniques. The TEM images (Fig. 6 a and b) show that FeNPs are successfully synthesized. According to the image in Fig. 6 a, the size of the synthesized single nanoparticle was about 40–80 nm; YL-FeNPs had irregular shapes, and the particles had a certain core–shell structure; the darker part inside the particle was mainly composed of a Fe core, and the outer light-colored part mainly consisted of organic substances of the extract. As shown in Fig. 6 b, YL-FeNPs exhibited a certain degree of agglomeration. The SEM image (Fig. 6c) shows that the surface of YL-FeNPs before Cr(VI) adsorption is relatively rough with pores of different sizes. After adsorption (Fig. 6d), some substances covered the surface of YL-FeNPs and filled the pores.

Figure 7 shows the FTIR spectra of YL-FeNPs before and after adsorption and of the extract for comparison. The broad bands at 3391 cm^{-1} in the extract and at 3370 cm^{-1} in YL-FeNPs before adsorption were attributed to O–H stretching vibrations of polyphenols [29, 30]. The peaks at 2925 cm^{-1} in both the extract and the YL-FeNPs before adsorption were assigned to C–H stretching vibrations [31]. The weak peaks at 1690 cm^{-1} in the extract and at 1689 cm^{-1} and 1648 cm^{-1} in YL-FeNPs before adsorption were attributed to C = O stretching vibrations of carboxyl groups [32–34]. C–H bending vibrations caused the peaks at 1456 cm^{-1} and 1454 cm^{-1} in the extract and in YL-FeNPs before adsorption, respectively [35, 36]. The weak peaks at 1046 cm^{-1} in the extract and at 1095 cm^{-1} in YL-FeNPs before adsorption were assigned to C–O stretching vibrations [37, 38].

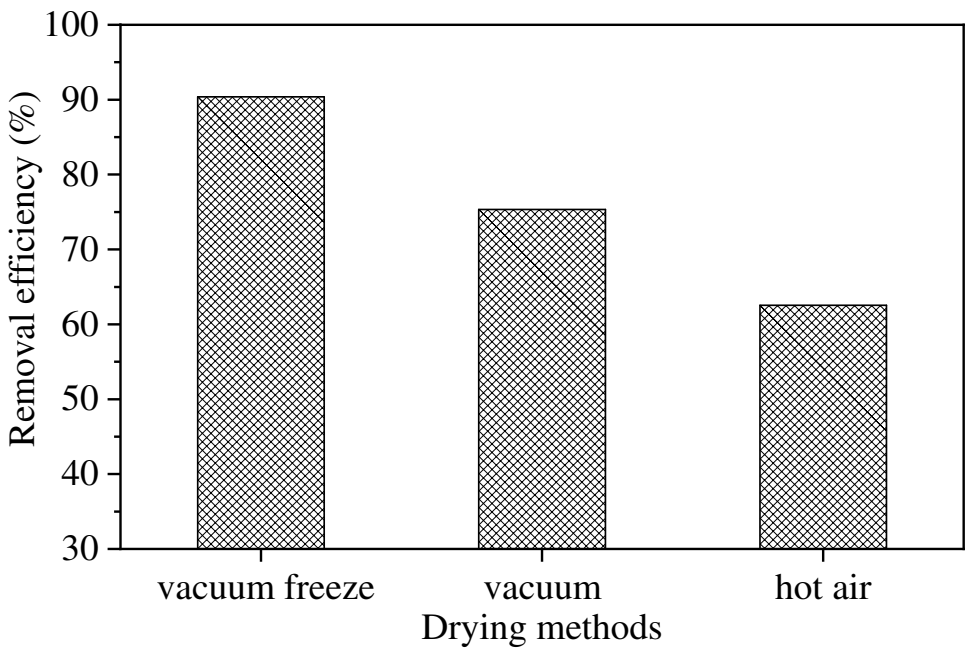

Fig. 5 Effect of drying methods on Cr(VI) removal (vacuum freeze: drying under vacuum at − 50 °C, vacuum: drying under a vacuum at 60 °C, hot air: hot-air drying at 60 °C)

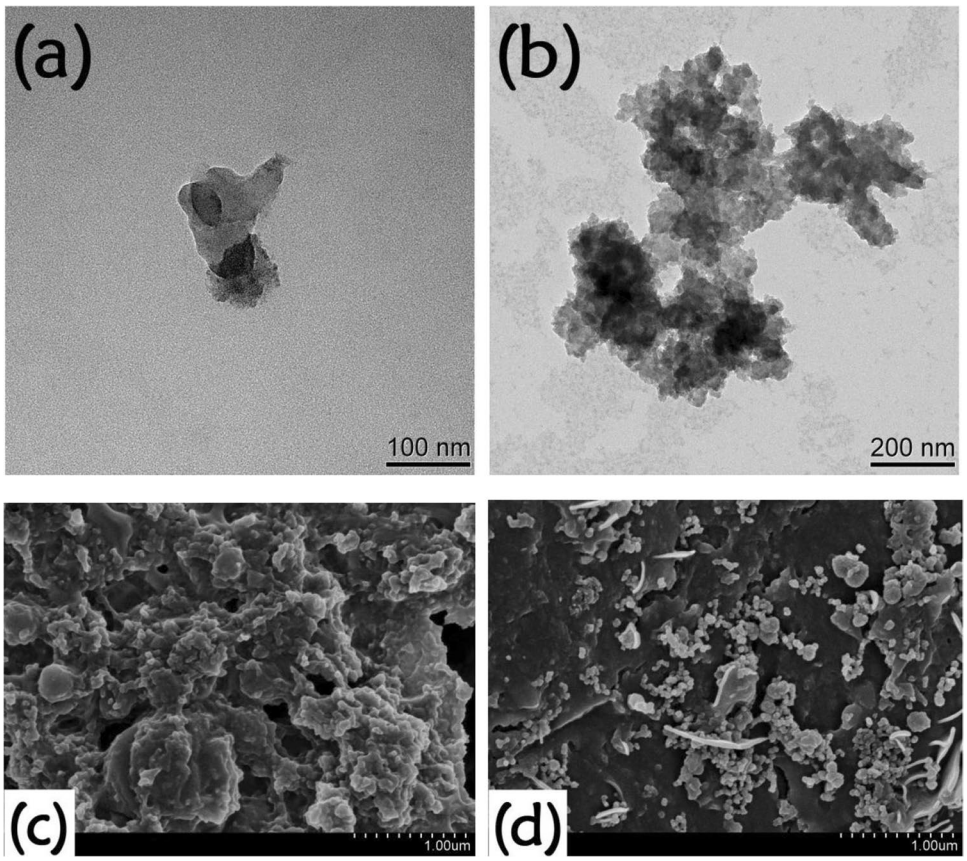

Fig. 6 TEM images of YL-FeNPs (**a**), (**b**); SEM images before (**c**) and after (**d**) Cr(VI) adsorption by YL-FeNPs

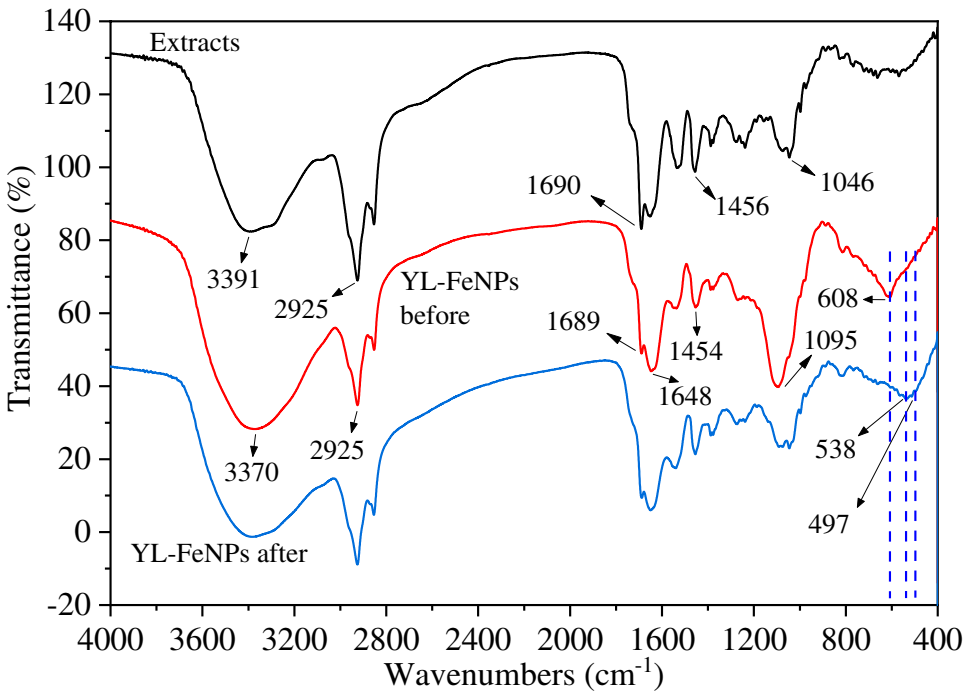

Fig. 7 FTIR spectra of Yali pear peel extracts and YL-FeNPs before and after hexavalent chromium adsorption

The band at 608 cm^{-1} in the latter material was attributed to Fe–O stretching vibration of Fe_3O_4 [39], which justified the formation of iron nanoparticles. The above analysis also indicates that the surface of YL-FeNPs is covered with polyphenols and other organic substances present in the extract, which is also consistent with the core–shell structure shown in Fig. 6 a.

The FTIR spectra of YL-FeNPs are different before and after hexavalent chromium adsorption. After adsorption, the intensity of the Fe–O peak at 608 cm^{-1} was significantly reduced, which may have been caused by the interaction between Fe–O and Cr(VI). The peak of O–Cr–O in Cr_2O_3 appeared at 538 cm^{-1} [40], and its presence in the spectrum after adsorption might be attributed to the reduction of Cr(VI) to Cr(III) which then attached to the surface of YL-FeNPs. A new weak peak near 497 cm^{-1} may be related to the complexation of Fe and Cr during the co-precipitation process [41, 42].

The XRD pattern of YL-FeNPs before adsorption is shown in Fig. 8, which exhibited no obvious diffraction peaks, showing that the YL-FeNP material is amorphous. The weak characteristic peak at about $2\theta = 35.6°$ is commonly attributed to Fe_2O_3, indicating that part of Fe(0) was oxidized during synthesis or drying. A zero-valent iron (α-Fe) diffraction peak and a Fe_3O_4 peak were discovered at approximately $2\theta = 44.5°$ and $2\theta = 28.5°$, respectively [43]. The weak peak at about $2\theta = 25°$ may represent organic materials originating from the extract.

The wide scan XPS spectrum of the YL-FeNPs shows peaks assigned to C1s, N1s, O1s, and Fe2p (Fig. 9a). The Fe2p narrow scan XPS spectrum is shown in Fig. 9b. The peak located at 711.0 eV was assigned to Fe^{3+}, while the binding energy of 709.3 eV was attributed to Fe^{2+}; the pattern is very similar to that of Fe_3O_4 detected in previous studies [44]. Therefore, the XPS test proved that YL-FeNPs contained Fe_3O_4. The weak peaks at about 707.1 eV and 719.8 eV represent Fe(0), indicating that YL-FeNPs contained a small amount of Fe(0). Since YL-FeNPs contacted with oxygen during the synthesis and drying process, the surface contained iron oxides. According to the analysis results of XPS, FTIR, and XRD, Fe_3O_4 and Fe(0) were the main forms of Fe in YL-FeNPs.

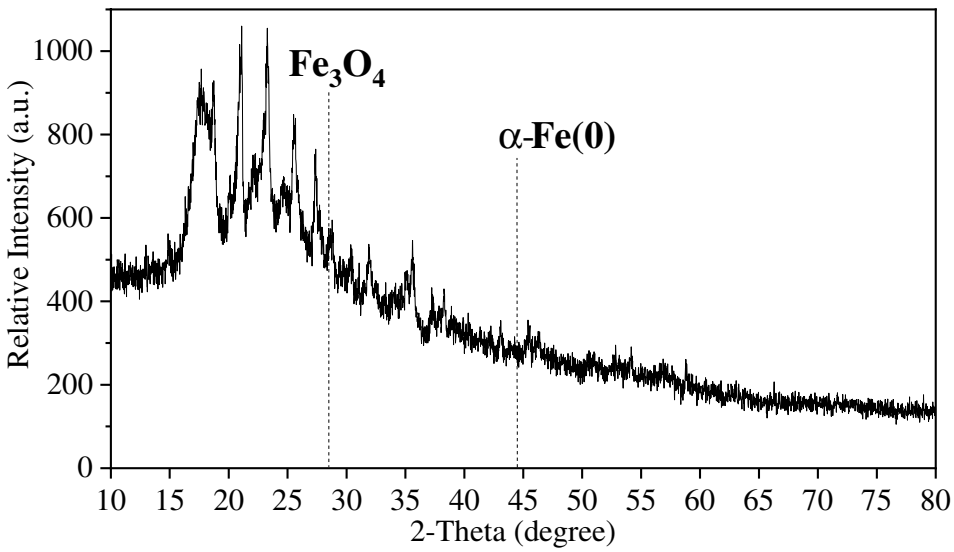

Fig. 8 XRD analysis of YL-FeNPs before adsorption

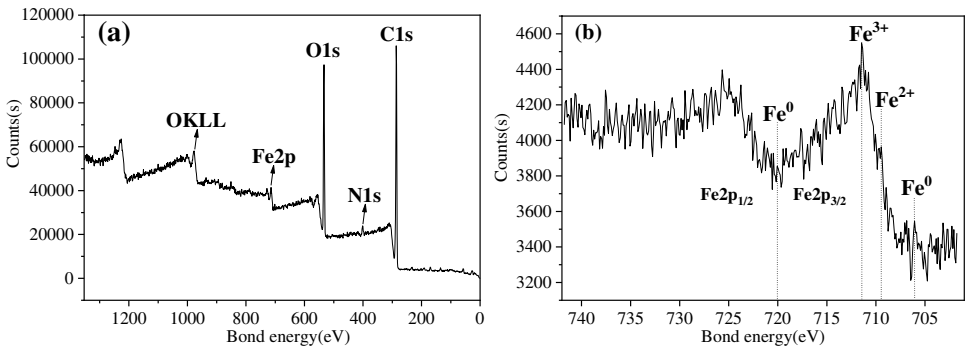

Fig. 9 Wide scan XPS spectrum (**a**) and Fe2p XPS spectrum (**b**) of YL-FeNPs

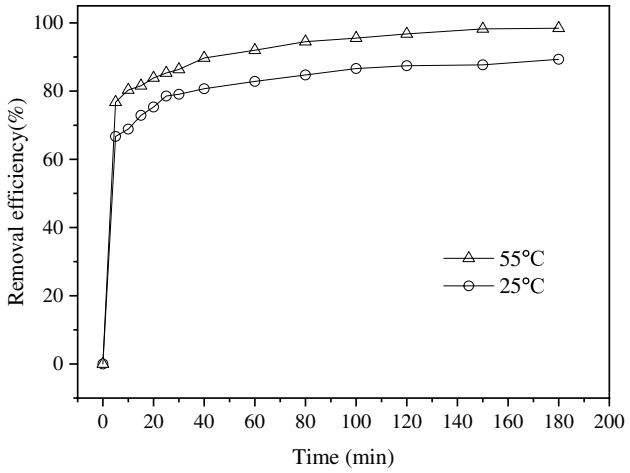

Fig. 10 Effect of contact time on Cr(VI) removal (initial Cr(VI) concentration: 12 mg/L, pH = 5) at adsorption temperatures of 25 °C and 55 °C

3.3 Application of YL-FeNPs for Cr(VI) removal

At an initial Cr(VI) concentration of 12 mg/L, the change in removal efficiency with contact time is shown in Fig. 10 for the temperatures of 25 °C and 55 °C. With the increase in contact time, the removal efficiency at both temperatures increased. In the first 5 min, the efficiency increased dramatically, reaching 66.7% at 25 °C and 76.8% at 55 °C; after 5 min, the removal efficiency improved slowly and basically reached equilibrium after 120 min with a Cr(VI) adsorption of 87.4% at 25 °C and of 96.8% at the higher temperature. In the first 5 min, the higher number of adsorption sites available on YL-FeNPs caused a fast increase in removal efficiency. Thereafter, the adsorption sites gradually reduced in number, and the removal efficiency increased slowly and gradually reached equilibrium.

The change in the removal efficiency with the initial Cr(VI) concentration is shown in Fig. 11 for adsorption at 25 °C and 55 °C. At the initial concentration of 10 mg/L, the removal efficiency was 91.6% at 25 °C and 99.3% at 55 °C and declined with increasing initial Cr(VI) concentration for both temperatures. At a concentration of 80 mg/L, the efficiency dropped to 14.5% and 21.6% for the lower and higher temperature, respectively. As evident from Figs. 10 and 11, the removal efficiency improved with the increase in temperature, which indicates that the adsorption of Cr(VI) by YL-FeNPs was an endothermic process.

The kinetics of Cr(VI) adsorption on YL-FeNPs was analyzed using pseudo-first-order and pseudo-second-order kinetics models (Table 1). In the equations of the model, q_e (mg·g^{-1}) and q_t (mg·g^{-1}) are the adsorption capacity of YL-FeNPs at equilibrium and at time t (min), respectively;

Table 1 The adsorption kinetics parameters for the removal of Cr(VI) by YL-FeNPs

Kinetic	Model	q_e (mg/g)	k_1 or k_2	R^2	T
First order	$q_t = q_e(1 - e^{-k_1 t})$	27.27	$k_1 = 0.3215$	0.943	55 °C
Second order	$q_t = \frac{k_2 q_e^2 t}{1 + k_2 q_e t}$	28.62	$k_2 = 0.0202$	0.981	55 °C

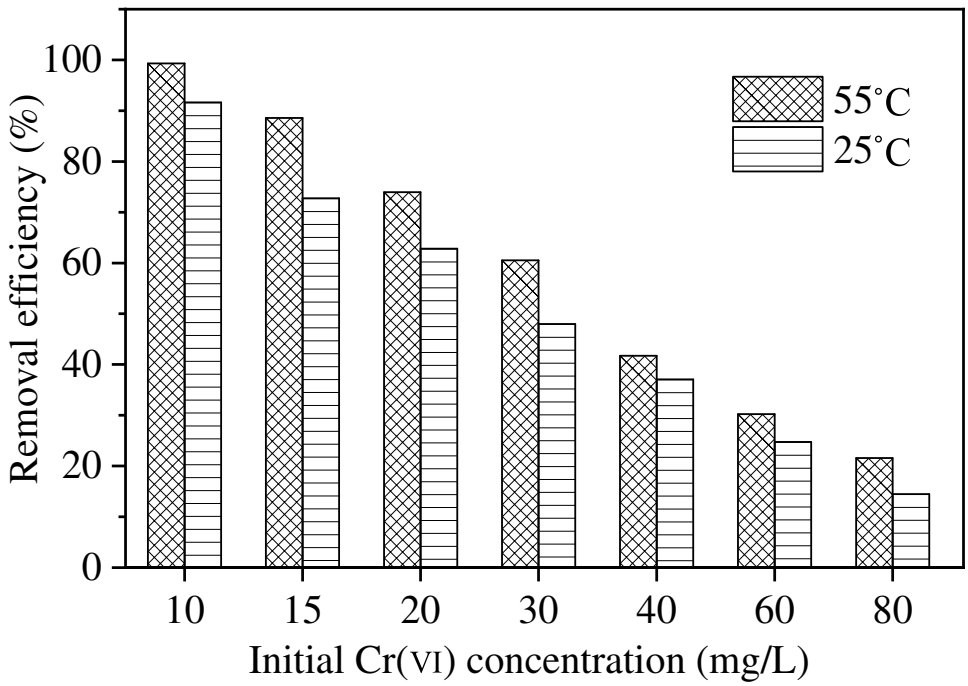

Fig. 11 Effect of initial Cr(VI) concentration on Cr(VI) removal (conditions: 0.02 g YL-FeNPs, pH = 5, 120 min contact time)

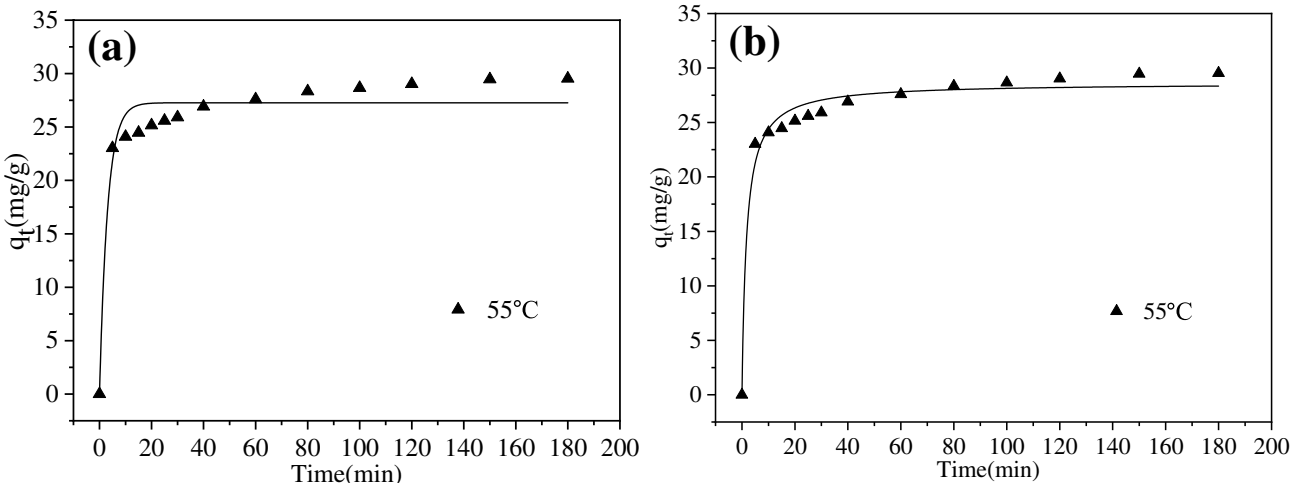

Fig. 12 Model data of pseudo-first-order (**a**) and pseudo-second-order (**b**) kinetics for Cr(VI) adsorption

k_1 (min^{-1}) and k_2 ($mg \cdot g^{-1} \cdot min^{-1}$) are the rate constants of the first-order and second-order models, respectively.

The fitting results of the two models are shown in Fig. 12 and Table 1. In the experiment, pH was 5, and the temperature was 55 °C. The correlation coefficient of the second-order model ($R^2 = 0.981$) was greater than that of the first-order model ($R^2 = 0.943$), and the deviation of the scattered points from the second-order model curve was smaller, indicating that the second-order model can better fit the adsorption process. At 55 °C, q_e was 28.62 mg/g, and the adsorption of hexavalent chromium by YL-FeNPs was dominated by chemisorption.

To study the relationship between equilibrium adsorption concentration and adsorption capacity, Langmuir and Freundlich isotherm models (Table 2) were used to analyze the adsorption data. In the equations of the models, C_e (mg/L) and q_e (mg/g) denote the equilibrium concentration and adsorption amount of Cr(VI) at equilibrium, respectively. K_L (L/mg) is the Langmuir constant. The variable q_m (mg/g) is the maximum amount of Cr(VI) adsorbed by YL-FeNPs. K_F [(mg/g)(L/mg)$^{1/n}$] and n are the Freundlich constants. R_L is the dimensionless constant separation factor used to describe the adsorption characteristics in the Langmuir model ($R_L = 1 / (1 + K_L \cdot C_0)$). C_0 (mg/L) in the formula is the initial concentration of hexavalent chromium. The adsorption process is unfavorable ($R_L > 1$), favorable ($0 < R_L < 1$), linear ($R_L = 1$), or irreversible ($R_L = 0$).

Adsorption equilibrium experiments were carried out at a pH of 5 and a temperature of 55 °C. The Langmuir (L) and Freundlich (F) models were used to analyze the adsorption isotherm results of Cr(VI) on YL-FeNPs. Figure 13 a and b show the experimental values and the linear fitting results of the L and F models, respectively. The L model exhibited a better fit, and the deviation of the scattered points from the fitted straight line was smaller compared to the F model. As listed in Table 2, the correlation coefficient of the L model ($R^2 = 0.9982$) was greater than that of the F model ($R^2 = 0.9068$). According to the L model, Cr(VI) adsorption occurred on the homogeneous surface of YL-FeNPs through monolayer sorption. The maximum adsorption capacity (Q_m) was determined as 43.99 mg/g. The value of R_L in Table 1 was in the range of 0.0052–0.0404, indicating that the adsorption at 55 °C was favorable.

The effect of different anions on the removal of Cr(VI) by YL-FeNPs is shown in Fig. 14. As the anion concentration increased from 0.5 to 2.0 mmol/L, the Cr(VI) adsorption

Table 2 Isotherm constants for Cr(VI) adsorption on YL-FeNPs

Isotherm model	Equation	Parameters	Values
Langmuir	$\frac{C_e}{q_e} = \frac{1}{q_m K_L} + \frac{C_e}{q_m}$	Q_m (mg/g)	43.99
		K_L (L/mg)	2.377
		R_L range	0.0052–0.0404
		R^2	0.9982
Freundlich	$\log q_e = \log K_F + \frac{1}{n} \log C_e$	K_F (mg/g)(L/mg)$^{1/n}$	32.18
		n	11.10
		R^2	0.9068

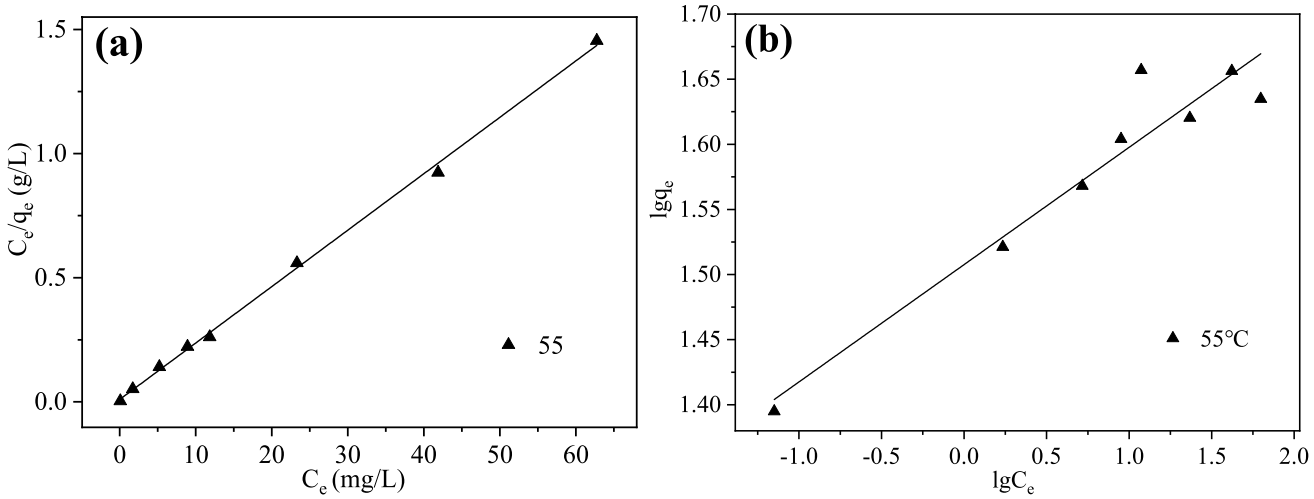

Fig. 13 Adsorption isotherms of Langmuir (**a**) and Freundlich (**b**) models for Cr(VI) adsorption on YL-FeNPs

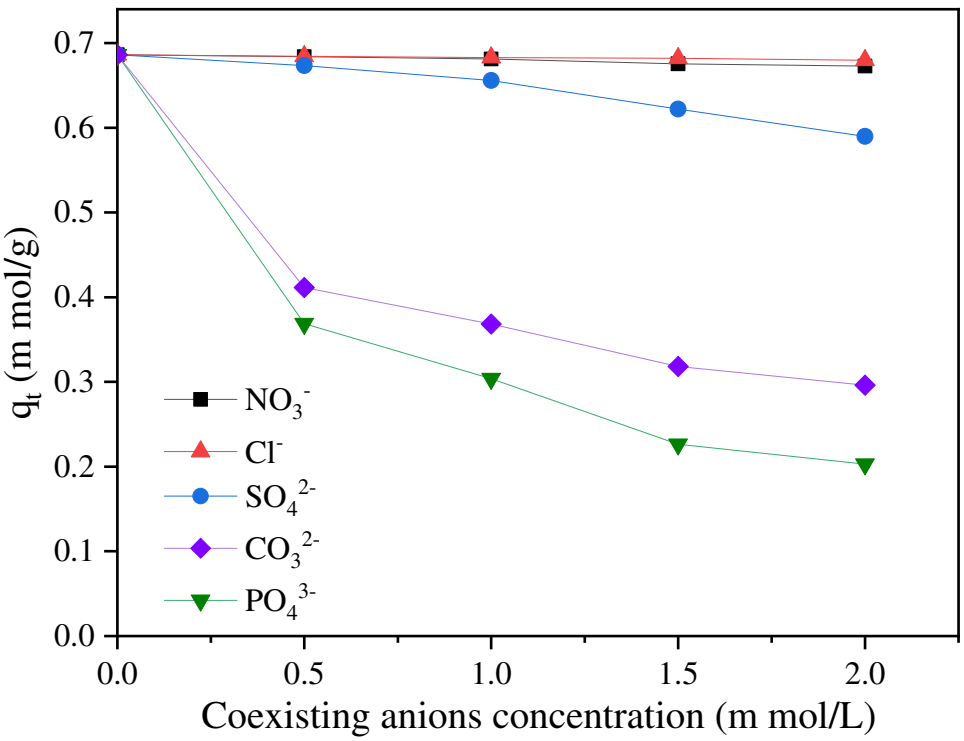

Fig. 14 Comparison of the effect of coexisting anions on Cr(VI) adsorption (conditions: 0.02 g YL-FeNPs, pH = 5, 55 °C, 120-min contact time)

capacity of YL-FeNPs (q_t) decreased to different extents, whereby NO_3^- and Cl^- demonstrated almost no influence on q_t. At an anion concentration of 0.5 mmol/L, the presence of PO_4^{3-}, CO_3^{2-}, and SO_4^{2-} reduced q_t by 46.3%, 40.0%, and 1.8%, respectively, and by 70.4%, 56.9%, and 14.0% as the anion concentration was increased to 2.0 mmol/L. The results indicate that YL-FeNPs can still remove Cr(VI) effectively at low anion concentrations. At a pH of 5, Cr(VI) in water mainly existed in the form of $HCrO_4^-$, and the added negatively charged anions carry on competition with $HCrO_4^-$ for the active sites on YL-FeNPs. Among the anions of the same molar concentration, PO_4^{3-} possessed the highest negative charge, while NO_3^- and Cl^- had the smallest negative charge. Therefore, PO_4^{3-} exhibited the greatest and NO_3^- and Cl^- the least impact on q_t.

The effect of real water bodies on the removal of Cr(VI) by YL-FeNPs is shown in Fig. 15. The adsorption experiments were conducted at 25 °C and the natural pH values of the water sources, which were 7.15, 8.53, and 8.17 for deionized water (D), river water (R), and tap water (T),

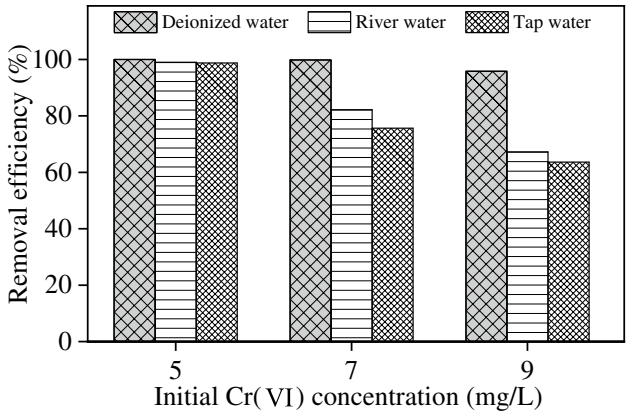

Fig. 15 Effect of deionized, river, and tap water on Cr(VI) removal (conditions: 0.02 g YL-FeNPs, natural pH, 25 °C, 120-min contact time)

respectively. When the initial Cr(VI) concentration was 5 mg/L, the removal efficiency in D, R, and T was 100%, 99%, and 98.8%, respectively, and decreased to 95.8%, 67.2%, and 63.6% when the initial Cr(VI) concentration changed to 9 mg/L. With decreasing pH value, the amount of H^+ on the surface of YL-FeNPs and, consequently, the adsorption of $HCrO_4^-$ increase; therefore, the removal efficiency was the highest in deionized water. Although the pH value of tap water (8.17) was lower than that of river water (8.53), tap water mainly contained inorganic salts, which may compete with hexavalent chromium for adsorption sites and thereby reduce the removal of Cr(VI); river water, however, contained low concentrations of organic compounds, which would promote the removal of Cr(VI) by the adsorbent [45]. Therefore, the removal efficiency was lower in tap water than in river water.

3.4 Reaction mechanism of Cr(VI) removal

According to previous research on the mechanism of Cr(VI) removal by green FeNPs [15, 19], the mechanism of Cr(VI) removal by YL-FeNPs is proposed as follows:

$$2HCrO_4^- + 3Fe^0 + 14H^+ \rightarrow 3Fe^{2+} + 2Cr^{3+} + 8H_2O \quad (3)$$

$$HCrO_4^- + 3Fe^{2+} + 7H^+ \rightarrow 3Fe^{3+}Cr^{3+}4H_2O \quad (4)$$

$$(1-x)Fe^{3+} + xCr^{3+} + 3H_2O \rightarrow (Cr_xFe_{1-x})(OH)_3 \downarrow +3H^+ \quad (5)$$

The mechanism mainly consists of three parts. (1) Adsorption: After YL-FeNPs are added to the Cr(VI) solution, Cr(VI) contacted the surface of the material due to electrostatic attraction and other reasons. (2) Reduction of Cr^{6+}: The results of FTIR, XRD, and XPS in this paper (Figs. 7, 8, and 9) have shown that YL-FeNPs contained Fe^0 and Fe^{2+}, and these Fe species reduced Cr^{6+} in the form of $HCrO_4^-$ to Cr^{3+} (Eqs. (3) and (4)) during the adsorption reaction, which is consistent with the peak of O–Cr–O in Cr_2O_3 after adsorption (Fig. 7); at the same time, Fe^0 and Fe^{2+} were finally oxidized to Fe^{3+} (Eqs. (3) and (4)), which is consistent with the apparent decrease in intensity of the Fe–O peak in Fe_3O_4 after adsorption (Fig. 7). (3) Co-precipitation: After adsorption, Cr^{3+} and Fe^{3+} formed precipitates in the form of Cr^{3+}/Fe^{3+} hydroxide such as $Cr_xFe_{1-x}(OH)_3$ (Eq. (5)), covering the surface of YL-FeNPs, which is consistent with the appearance of the complexation peak of Fe and Cr near 497 cm^{-1} after adsorption (Fig. 7) and the TEM image after adsorption (Fig. 6d). In addition, the adsorption kinetics analysis (Fig. 12 and Table 1) shows that the adsorption process was dominated by chemisorption, which is also consistent with the chemical reaction mechanism indicated by Eqs. (3), (4), and (5).

4 Conclusions

In this paper, Yali pear peel extracts as reducing agents and $FeSO_4$ were used to successfully synthesize YL-FeNPs for the first time. The optimized synthesis conditions are as follows: 27 g of pear peel was extracted in 360 mL of 50 vol% ethanol solution in water at 80 °C for 60 min, the Fe^{2+}-extract ratio was 1:1, and vacuum freeze drying was applied as the drying method. According to the characterization results, the optimized YL-FeNPs had a particle size of about 40–80 nm, a core–shell structure, and an irregular shape; partial pores with a certain degree of aggregation were present on the surface. The main components of YL-FeNPs were Fe_3O_4 and Fe^0. As the initial Cr(VI) concentration decreased and the adsorption temperature increased, the Cr(VI) removal efficiency of YL-FeNPs increased. The adsorption of Cr(VI) basically reached equilibrium within 2 h. The removal efficiency of 12 mg/L Cr(VI) by YL-FeNPs at 55 °C was 96.8%. The adsorption data conformed to the Langmuir isotherm model, and the maximum adsorption capacity (Q_m) at 55 °C was 43.99 mg/g. When the concentration of coexisting anions was low, YL-FeNPs also showed good adsorption performance in real natural water.

Funding This work was supported by the Science and Technology Support Plan for Youth Innovation of Colleges and Universities in Shandong Province (2020KJD005), the Humanities and Social Sciences Research Project of the Ministry of Education in China (19YJCZH134).

Declarations

Conflict of interest The authors declare no competing interests.

References

1. Yan L, Dong F, Lin X, Zhou X, Kong L, Chu W, Diao Z (2021) Insights into the removal of Cr(VI) by a biochar-iron composite from aqueous solution: reactivity, kinetics and mechanism. Environ Technol Inno. 24:102057
2. Diao Z, Xu X, Jiang D, Kong L, Sun Y, Hu Y, Hao Q, Chen H (2016) Bentonite-supported nanoscale zero-valent iron/persulfate system for the simultaneous removal of Cr(VI) and phenol from aqueous solutions. Chem Eng J 302:213–222
3. Dong F, Yan L, Zhou X, Huang S, Liang J, Zhang W, Guo Z, Guo P, Qian W, Kong L, Chu W, Diao Z (2021) Simultaneous adsorption of Cr(VI) and phenol by biochar-based iron oxide composites in water: Performance, kinetics and mechanism. J Hazard Mater 416:125930
4. Diao Z, Xu X, Chen H, Jiang D, Yang Y, Kong L, Sun Y, Hu Y, Hao Q, Liu L (2016) Simultaneous removal of Cr(VI) and phenol by persulfate activated with bentonite-supported nanoscale zero-valent iron: reactivity and mechanism. J Hazard Mater 316:186–193
5. Qian W, Liang J, Zhang W, Huang S, Diao Z (2022) A porous biochar supported nanoscale zero-valent iron material highly efficient for the simultaneous remediation of cadmium and lead contaminated soil. J Environ Sci 113:231–241
6. Diao Z, Du J, Jiang D, Kong L, Huo W, Liu C, Wu Q, Xu X (2018) Insights into the simultaneous removal of Cr^{6+} and Pb^{2+} by a novel sewage sludge-derived biochar immobilized nanoscale zero valent iron: coexistence effect and mechanism. Sci Total Environ 642:505–515
7. Diao Z, Yan L, Dong F, Chen Z, Guo P, Qian W, Zhang W, Liang J, Huang S, Chu W (2021) Ultrasound-assisted catalytic reduction of Cr(VI) by an acid mine drainage based nZVI coupling with FeS_2 system from aqueous solutions: performance and mechanism. J Environ Manage 278:111518
8. Mokrzycki J, Michalak I, Rutkowski P (2021) Biochars obtained from freshwater biomass-green macroalga and hornwort as Cr(III) ions sorbents. Biomass Conv Bioref 11:301–313
9. Cigeroglu Z (2021) Preparation of $ZnO/BaTiO_3$ adsorbent using Elaeagnus Angustifolia L. leaf extract and its evaluation for ciprofloxacin removal from aqueous solutions: an optimization study. Biomass Conv Bioref 11:1407–1417
10. Jagwani D, Krishna PH (2021) Nature's nano-assets: green synthesis, characterization techniques and applications – a graphical review. Mater Today 46:2307–2317
11. Salmani MH, Abedi M, Mozaffari SA, Mahvi AH, Sheibani A, Jalili M (2021) Simultaneous reduction and adsorption of arsenite anions by green synthesis of iron nanoparticles using pomegranate peel extract. J Environ Health Sci Engineer 19:603–612
12. Lingamdinne LP, Vemula KR, Chang YY, Yang JK, Karri RR, Koduru JR (2020) Process optimization and modeling of lead removal using iron oxide nanocomposites generated from biowaste mass. Chemosphere 243:125257
13. Machado S, Grosso JP, Nouws HP, Albergaria JT, Delerue MC (2014) Utilization of food industry wastes for the production of zero-valent iron nanoparticles. Sci Total Environ 496:233–240
14. Ting AS, Chin JE (2020) Biogenic synthesis of iron nanoparticles from apple peel extracts for decolorization of malachite green dye. Water Air Soil Poll 231:278
15. Mystrioti C, Sparis D, Papasiopi N, Xenidis A, Dermatas D, Chrysochoou M (2015) Assessment of polyphenol coated nano zero valent iron for hexavalent chromium removal from contaminated waters. Bull Environ Contam Toxicol 94:302–307
16. Harshiny M, Iswarya CN, Matheswaran M (2015) Biogenic synthesis of iron nanoparticles using Amaranthus dubius leaf extract as a reducing agent. Powder Technol 286:744–749
17. Liu Y, Jin X, Chen Z (2018) The formation of iron nanoparticles by Eucalyptus leaf extract and used to remove Cr(VI). Sci Total Environ 627:470–479
18. Akhbari M, Hajiaghaee R, Ghafarzadegan R, Hamedi S, Yaghoobi M (2019) Process optimisation for green synthesis of zero-valent iron nanoparticles using Mentha piperita. IET Nanobiotechnol 13:160–169
19. Wei Y, Fang Z, Zheng L, Tsang EP (2017) Biosynthesized iron nanoparticles in aqueous extracts of Eichhornia crassipes and its mechanism in the hexavalent chromium removal. Appl Surf Sci 399:322–329
20. Wei Y, Fang Z, Zheng L, Tan L, Tsang EP (2016) Green synthesis of Fe nanoparticles using Citrus maxima peels aqueous extracts. Mater Lett 185:384–386
21. Pan Z, Lin Y, Sarkar B, Owens G, Chen Z (2020) Green synthesis of iron nanoparticles using red peanut skin extract: synthesis mechanism, characterization and effect of conditions on chromium removal. J Colloid Interf Sci 558:106–114
22. Wu Y (2018). Removal of U(VI) from aqueous solution using green synthesized iron nanoparticles supported on bentonited. Master Dissertation. Univ S China, Hengyang, China.
23. Liu Y (2018). Green synthesis of iron-based nanoparticles by *eucalyptus* leaf and used to remove Cr(VI) from aqueous solutions. Master Dissertation. Fujian Norm Univ, Fuzhou, China.
24. Hao R, Li D, Zhang J, Jiao T (2021) Green synthesis of iron nanoparticles using green tea and its removal of hexavalent chromium. Nanomaterials 11:650
25. Deng Q, Luo S, Tong Z, Wang Y, Wang Z, Fan C (2020) Green synthesis of shell-supported nano zero-valent iron using mango peer extract and the application for removal of methyl orange. J Henan Norm Univ (Nat Sci Edit) 48:64–72
26. Geng ZH, Qin WD, Ma LH, Zhang ZS (2009) Study on optimization of extraction technology of polyphenols in pear peel. Sci Technol Food Ind 30:233–235
27. Zhao M, Zhang SL, Qi KJ, Heng YJ, Tao ST (2013) Optimization of extraction of polyphenols from pear fruitlet pulp and analysis of its composition. Sci Technol Food Ind 34:268–271
28. Liu H, Yin C, Wei XY, Li JH, Li T, Wang F (2015) Influence of drying methods on the structure and property of regenerated nanocellulose. N Chem Mater 2:184–187
29. Chaudhuri SK, Malodia L (2017) Biosynthesis of zinc oxide nanoparticles using leaf extract of Calotropis gigantea: characterization and its evaluation on tree seedling growth in nursery stage. Appl Nanosci 7:501–512
30. Jin KC, Do KL, Yong WK, Byoung RM, Jong HK (2008) Composite polymer electrolyte membranes comprising triblock copolymer and heteropolyacid for fuel cell applications. J Polym Sci Pol Phys 46:691–701
31. Kenawy ER, Ghfar AA, Wabaidur SM, Khan MA, Siddiqui MR, Alothman ZA, Alqadami AA, Hamid M (2018) Cetyltrimethylammonium bromide intercalated and branched polyhydroxystyrene functionalized montmorillonite clay to sequester cationic dyes. J Environ Manage 219:285–293
32. Jeyakumar P, Saravanakumar SS, Kulathuraan K, Ramadas V (2015) Functionalization of biomolecules with nanostructured porous silicon for biomedical application. Surf Rev Lett 22(2):1550022
33. Dega-Szafran Z, Dutkiewicz G, Kosturkiewicz Z, Szafran M (2008) Structure of complex of N-methylpiperidine betaine with p-hydroxybenzoic acid studied by X-ray, FTIR and DFT methods. J Mol Struct 875:346–353
34. Bouyanfif A, Liyanage S, Hequet E, Moustaid MN, Noureddine A (2019) Fourier transform infrared microspectroscopy detects biochemical changes during C. elegans lifespan. Vib Spectrosc 102:71–78

35. Masood F, Aziz M, Haider H, Shakil O, Yasin T, Hameed A (2018) Biodegradation of gamma irradiated poly-3-hydroxybutyrate/sepiolite nanocomposites. Int Biodeter Biodegr 126:1–9
36. Severcan F, Toyran N, Kaptan N, Turan B (2000) Fourier transform infrared study of the effect of diabetes on rat liver and heart tissues in the C-H region. Talanta 53:55–59
37. Zhang Z, Tahir N, Li Y, Zhang T, Zhu S, Zhang Q (2019) Tailoring of structural and optical parameters of corncobs through ball milling pretreatment. Renew Energ 141:298–304
38. Wanasekara ND, Santos RP, Douch C, Frollini E, Eichhorn SJ (2016) Orientation of cellulose nanocrystals in electrospun polymer fibres. J Mater Sci 51:218–227
39. Goncalves NS, Horn A, Lanznaster M, Noda LK, Neves A (2006) Resonance raman spectroscopy of $Fe^{II}Fe^{III}$ and $Fe^{III}Fe^{III}$ model complexes containing an unsymmetrical dinucleating ligand: a biomimetic redox pair for uteroferrin. J Braz Chem Soc 17:1658–1663
40. Li S, Wen X, Liu C, Dai Y, Shi X, Li L, Tan S, Qu Q, Huang R (2021) A sustainable way to reuse Cr(VI) into an efficient biological nanometer electrocatalyst by Bacillus megaterium. J Hazard Mater 409:124942
41. Qian L, Liu S, Zhang W, Chen Y, Ouyang D, Han L, Yan J, Chen M (2019) Enhanced reduction and adsorption of hexavalent chromium by palladium and silicon rich biochar supported nanoscale zero-valent iron. J Colloid Interf Sci 533:428–436
42. Liu Q, Xu M, Li F, Wu T, Li Y (2016) Rapid and effective removal of Cr(VI) from aqueous solutions using the $FeCl_3/NaBH_4$ system. Chem Eng J 296:340–348
43. Li M, Tian Y, Li S, Guo B (2018) Optimization of Removal of Cr(VI) from aqueous solution by green synthesis of zero-valent iron nanoparticles by response surface methodological analysis and its kinetic study. China Rural Water and Hydropower 8:113–118
44. Krishnamoorthy S, Ajala F, Mohammed SM, Asok A, Shukla S (2021) High adsorption and high catalyst regeneration kinetics observed for Flyash-Fe_3O_4-Ag magnetic composite for efficient removal of industrial azo reactive dyes from aqueous solution via persulfate activation. Appl Surf Sci 548:149265
45. Yang G (2015) Synthesis of magnetic mesoporous carbon and its application in remediation of water pollution. Master Dissertation. Hunan Univ, Changsha, China.